RSC Advances

PAPER

View Article Online
View Journal | View Issue

Cite this: *RSC Adv.*, 2021, **11**, 36222

Formation and enhancement of negative thermal quenching in emission of $KGdF_4:Eu^{3+}$, Yb^{3+}@GQDs†

Zhigao Wu,[ac] Chang Chen,[b] Yaxiong Wang,[b] Chaolian Luo,[b] Sen Liao,*[ab] Yingheng Huang*[ab] and Junyu Ming*[b]

Received 6th October 2021
Accepted 2nd November 2021

DOI: 10.1039/d1ra07413j

rsc.li/rsc-advances

In order to obtain a red emitting phosphor with good luminescence thermal stability, a series of $KGdF_4:Eu^{3+}$, Yb^{3+}@GQD (GQD: Cl-containing graphene quantum dots) red emitting phosphors have been synthesized by the co-precipitation method, and their luminescence thermal properties have also been studied in detail. It is intriguing that the negative thermal quenching (NTQ) effect is induced by the double doping of Yb^{3+}, and the effect is further enhanced by GQD coating. The strongest integrated PL intensities of the optimal double doped sample and the optimal GQD-coated sample are at 130 and 170 °C, in which the corresponding integrated PL intensities are presented as 117.7 and 156.5% of the initial value at 30 °C, respectively. The NTQ effect makes the optimal GQD coated sample have good luminescent thermal stability, so it can be applied for high-power WLEDs. A mechanism of energy conversion from heat to light is discussed and suggested for the effect.

1. Introduction

White light emitting diodes (WLEDs) have gradually become the mainstream lighting source due to their characteristics of high efficiency, low energy consumption, low heat dissipation, long life, good light quality, energy saving and environmental protection.[1–3] The traditional method to obtain white light is to coat the yellow emitting phosphor on the blue LED chip, and realize the white light emission by mixture of the blue light of the chip and the yellow light of the phosphor. But there are some serious problems in this system, such as thermal quenching, poor color reproducibility, high color temperature (CCT > 5000 K), and low color rendering index (CRI < 80) due to the lack of red emitting components, which have a great impact on practical application.[4–6] Another method to obtain white light is to coat three primary color (blue, yellow and red color) phosphors on near-ultraviolet (near-UV) light LED chip (370–410 nm) and achieve white light emission by mixture of the three primary color lights. The phosphors are the focus of current research on luminescent materials. However, the red emitting phosphors obtained in this way are mainly $Y_2O_2S:Eu^{3+}$. Their luminescent efficiency is far lower than that of blue and green phosphors and their chemical properties are unstable. It decomposes easily at WLEDs working temperatures to release toxic hydrogen sulfide and reduce the service life of WLEDs.[7] Therefore, it is urgent to develop a red emitting phosphor with high luminescent thermal stability, which is suitable for WLEDs excited by near-UV light (370–410 nm).

Eu^{3+} ion is generally recognized as a good activator for red phosphor. Under near-UV (370–410 nm) excitation, $^5D_0 \rightarrow {}^7F_j$ (j = 0, 1, 2, 3, 4) transitions emit red light, so that many researchers are trying to develop Eu^{3+} as activator to develop red emitting phosphor. But because of the shielding effect of 5s and 5p electrons in the outer shell, Eu^{3+} has weak luminescent intensity and small absorption cross section. So it is necessary to find an appropriate sensitizer to improve the luminescence intensity.[8–34] Eu^{3+} and Yb^{3+} often co-doped in various kinds of matrix, for example: Lu_2O_3,[13] CaF_2,[14] Gd_2O_3,[15] $KGdF_3$ (ref. 16) and $NaYF_4$,[17] *etc.*, and emission of Eu^{3+} is enhanced by absorbing the infrared light though Yb^{3+}. But, as best as we know, that under near-UV (370–410 nm) excitation, the emission enhancement of Eu^{3+} by co-doping of Yb^{3+} has been rarely reported.

In addition to luminescent intensity, thermal quenching of phosphors is also an important factor affecting the luminescent performance, and the Eu^{3+} doped red emitting phosphors are no exception. The luminescent intensity of Eu^{3+} will decrease with the increase of temperature in most matrices, such as $Ba_3Bi(PO_4)_3:Eu^{3+}$,[18] $Sr_2Al_3O_6F:Eu^{3+}$,[19] $K_4CaSi_3O_9:Eu^{3+}$,[20] $Ca_2LaTaO_6:Eu^{3+}$,[21] $Ba_3ZrNb_4O_{15}:Eu^{3+}$.[22] There are only a few reports to show that emission of Eu^{3+} can produce NTQ with the increase of temperature. For example, emission intensity of $K_5Y(P_2O_7):Eu^{3+}$ (ref. 23) increases with the increase of temperature before 100 °C, and emission intensity of $Ca_{18}Li_3Bi_{0.4}Eu_{0.6}(PO_4)_{14}:Eu^{3+}$ (ref. 24) at 60 °C is 230.4% of that initial value at

[a]School of Chemistry and Chemical Engineering, Guangxi University, Nanning, Guangxi, 530004, China. E-mail: liaosen@gxu.edu.cn; huangyingheng@163.com; Fax: +86 771 3233718; Tel: +86 771 3233718

[b]School of Resources, Environment and Materials, Guangxi University, Nanning, Guangxi, 530004, China. E-mail: 2945539376@qq.com

[c]School of Medicine and Health, Guangxi Vocational & Tecnnical Institute of Industry, Nanning, Guangxi, 530001, China

† Electronic supplementary information (ESI) available. See DOI: 10.1039/d1ra07413j

Table 1 ICP element analysis results of samples (i–iii)[a]

No.	K/%	Gd/%	Eu/%	Yb/%	Atomic ratios of K : Gd : Eu : Yb	Calculated molecular formulae
(i)	14.327	46.455	11.237	0.000	0.996 : 0.803 : 0.201 : 0.0000	KGF:0.20Eu^{3+}
(ii)	14.311	46.172	11.068	0.146	0.995 : 0.798 : 0.198 : 0.0023	KGF:0.20Eu^{3+}, 0.002Yb^{3+}
(iii)	14.354	46.149	10.957	0.134	0.998 : 0.798 : 0.196 : 0.0021	KGF:0.20Eu^{3+}, 0.002Yb^{3+}@GQDs$_{2\ mg\ mol^{-1}}$

[a] (i) KGF:0.20Eu^{3+}, (ii) KGF:0.20Eu^{3+}, 0.002Yb^{3+}, (iii) KGF:0.20Eu^{3+}, 0.002Yb^{3+}@GQDs$_{2\ mg\ mol^{-1}}$.

30 °C. Therefore, more studies are needed to improve the thermal stability of the Eu^{3+} doped phosphors.

In our previous work,[33] it has been reported that $KGdF_4$:Eu^{3+}:Sm^{3+} phosphor was induced to have the NTQ effect by coating with GQDs. It's implied that after Eu^{3+} and different rare earth ions co-doped phosphors are coated with GQDs, they may also have the NTQ effect. Rare earth fluoride of $KGdF_4$ is considered to be a good matrix due to its high ionicity, low phonon energy, good optical stability and high refractive index. So, it is widely used as matrix for various down-conversion and up-conversion materials.[27–30]

In addition, the ionic radius difference between Gd^{3+} and Eu^{3+} or Yb^{3+} is within 15%. Based on the Vegard Law,[7] the metal ion radius does not exceed 15%, they can easily replace each other, which facilitates co-doping of Eu^{3+} and Yb^{3+}. Therefore, $KGdF_4$ is a good matrix for doping of Eu^{3+} ion.

So, as a part of our system research, in this paper, based on $KGdF_4$:Eu^{3+}, Yb^{3+} obtained *via* a co-precipitation method, GQDs is coated on the surface of $KGdF_4$:Eu^{3+}, Yb^{3+} to form $KGdF_4$:Eu^{3+}, Yb^{3+}@GQDs hybrid composite luminescent materials. Some novel effects induced by co-doping of Yb^{3+} and coating of GQDs have been observed, which the NTQ effect was formed after co-doping of Yb^{3+} and it was further obviously enhanced by coating of GQDs.

2. Experimental procedure and methods

Experimental section is described in ESI.† Experimental section includes reagents, apparatus, and synthesis of the samples. Properties of GQDs are also described in (Table 1S, and Fig. 1S–6S†).

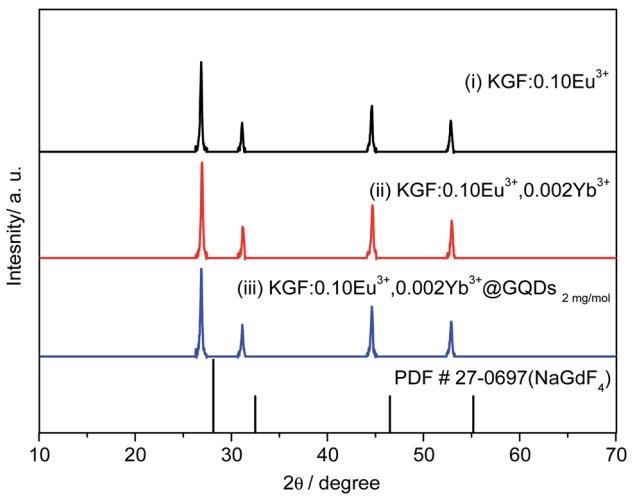

Fig. 1 XRD patterns of samples, (i) KGF:0.20Eu^{3+}; (ii) KGF:0.20Eu^{3+}, 0.002Yb^{3+}; (iii) KGF:0.20Eu^{3+}, 0.002Yb^{3+}@GQDs$_{2\ mg\ mol^{-1}}$.

3. Results and discussion

3.1 Structure, morphology and composition

The ICP elemental analysis data of samples (i–iii) are listed in Table 1, which the corresponding molecular formulae of the samples (i–iii) are KGF:0.20Eu^{3+}, KGF:0.20Eu^{3+}, 0.002Yb^{3+}, KGF:0.20Eu^{3+}, 0.002Yb^{3+}@GQDs$_{2\ mg\ mol^{-1}}$, respectively.

Fig. 1 shows the XRD patterns of the samples (i–iii) ((i) KGF:0.20Eu^{3+}, (ii) KGF:0.20Eu^{3+}, 0.002Yb^{3+}, (iii) KGF: 0.20Eu^{3+}, 0.002Yb^{3+}@GQDs$_{2\ mg\ mol^{-1}}$) and the standard spectra of $NaGdF_4$. Indexed results of Fig. 1 are listed in Table 2, which the crystal structures of all the three samples are identical to be close to that of cubic $NaGdF_4$ (space group $Fm\bar{3}m$ (225), PDF # 27-0697), which are supported by other authors' reports.[34–38] It can be seen from Fig. 1 and Table 2 that: first, doping of Eu^{3+}, Yb^{3+} and coating of GQDs do not change the structure of the samples. Second, the crystallinity of the samples is relatively high, and there is no any other impurity peaks. Finally, the crystal structures of the samples are similar to the standard pattern of cubic $NaGdF_4$(PDF # 27-0697), but the position of the all peaks are shifted to a small angle, due to the ionic radius of K^+ being larger than that of Na^+.[28,35–38]

In order to confirm the phase of the samples (i–iii), we not only synthesized $NaGdF_4$:0.20Eu^{3+} by the same method (Fig. 7S†), but also compared with the XRD patterns of $KGdF_4$:Ln^{3+} (Ln = Eu, Ce, Sm, Tb) reported by other authors.[34–38] Fig. 7S† shows that XRD pattern of the as-synthesized $NaGdF_4$:0.20Eu^{3+} is in agreement with those of hexagonal $NaGdF_4$ (PDF # 27-0699) and hexagonal $NaEuF_4$ (PDF # 49-1897), but it does not match to that of cubic $NaGdF_4$ (PDF # 27-0697).

Some authors illustrate that the XRD patterns of $KGdF_4$: Ln^{3+} (Ln = Eu, Ce, Sm, Tb)[34–38] are close to those of hexagonal $YGdF_4$ (PDF # 27-0466), cubic $NaYF_4$ (PDF # 06-0342), cubic $NaGdF_4$ (PDF # 27-0697), but they are not similar to that of orthorhombic $KGdF_4$ (PDF # 33-1007). It is interesting that the XRD patterns of the samples (i–iii) are the same as those of $KGdF_4$: Ln^{3+} (Ln = Eu, Ce, Sm, Tb),[34–38] indicating that they are phase of $KGdF_4$.

Fig. 2 shows the SEM image, EDS, XPS and FTIR spectra of sample (iii), KGF: 0.20Eu^{3+}, 0.002Yb^{3+}@GQDs$_{2\ mg\ mol^{-1}}$. Fig. 2a (SEM) shows that the sample is cluster of irregular particles with a size of about 5–10 μm, and many small particles are adsorbed on the cluster surface. Fig. 2b (EDS) shows that the sample contains elements of K, Gd, Eu, Yb, F and C, indicating that GQDs has been successfully coated on surface of the sample. XPS results (Fig. 2c) show that the sample is composed with K, Ti, Mn, F, C and O, which C and O come from GQDs, adsorbed CO_2 and H_2O, respectively. FTIR spectra (Fig. 2d) show that sample (iii) and GQDs have the same characteristic FTIR absorption peak (Fig. 6S†). Here,

Table 2 Lattice parameters and volumes of samples (i–iii)[a]

Sample	$a = b = c$/Å	Vol./Å^3
(i)	5.748	189.93
(ii)	5.740	189.18
(iii)	5.751	190.23
PDF # 027-0697	5.518	168.01

[a] (i) KGF:0.20Eu^{3+}, (ii) KGF:0.20Eu^{3+}, 0.002Yb^{3+}, (iii) KGF:0.20Eu^{3+}, 0.002Yb^{3+}@GQDs$_{2\ mg\ mol^{-1}}$.

the characteristic sharp peak at 1639 and 3450 cm^{-1} can be attributed to C=C vibration of GQDs, and O–H vibration of H_2O,[39] confirming that surface of the sample has GQDs. In conclusion, results of EDS, FTIR and XPS all illustrate that GQDs has been coated on the surface of the sample (iii).

3.2 Luminescence properties

Fig. 3 shows luminescent properties of the three samples at room temperature. As shown in Fig. 3a, the strongest excitation peaks of the samples are at about 393 nm. Co-doping of Yb^{3+} and coating of GQDs significantly enhances and widens the peaks, and the intensity order of the peaks is (iii) > (ii) > (i). Fig. 3b shows PL spectra of the samples, which the emission intensities are also significantly enhanced by Yb^{3+} co-doping and GQDs coating, but the position of the main emission peaks has not changed: (a) emission peak intensity of the sample (ii) is 1.40 times that of the sample (i); (b) emission peak intensity of sample (iii) is approximately 1.20 times that of the sample (ii) and approximately 1.68 times that of the sample (i). (c) It can be seen from Fig. 4Sb,† GQDs should have an emission peak at about 460 nm under excitation of 393 nm. However, in Fig. 3b, no emission peak of GQDs appears at about 460 nm, indicating that GQDs transfers energy to Eu^{3+} after absorbing excitation light. Decay curves of the samples (i) and (iii) are shown in Fig. 3c, which can be fitted with linear functions (here, the nonlinear equation of $y = A_1^* \exp(-x/\tau) + y_0$ is transformed into the linear equation of $\mathrm{Ln}(y - y_0) = A_1 - x/\tau$). Lifetimes of the samples (i–iii) obtained from the curves are 5.22, 5.90 and 6.28 ms, respectively. Fig. 3d shows chromaticity diagrams of the samples (i–iii), and corresponding CIE chromaticity coordinates are as follows: (i) (0.6156, 0.3839); (ii) (0.6150, 0.3845); (iii) (0.6147, 0.3848). Fig. 3d further shows that the three points have overlapped as one point, indicating the emissions of the samples have almost the same red color.

3.3 Luminescent properties at different concentrations of Eu^{3+}, Yb^{3+} and GQDs

Fig. 4a shows PL spectra of KGF:xEu^{3+}. All KGF:xEu^{3+} samples show similar PL spectra with different relative intensities. Three strong peaks observed at 591, 611, 650 and 700 nm are attributed to the $^5D_0 \rightarrow {}^7F_1$, $^5D_0 \rightarrow {}^7F_2$, $^5D_0 \rightarrow {}^7F_3$ and $^5D_0 \rightarrow {}^7F_4$ transitions of Eu^{3+} ion, respectively.[9,11] In addition, the weak peaks at 533, 552, 578, and 625 nm (shoulder peak) belong to the $^5D_1$–$^7F_1$, $^5D_1$–$^7F_2$, $^5D_1$–$^7F_3$ and $^5D_1$–$^7F_4$, respectively.[9] Curve of the emission intensity at 592 nm changes with different x is a parabola, achieves its summit when x is about 0.20.

Fig. 4b shows the emission spectra (PL) of KGF:0.20Eu^{3+}, yYb^{3+} samples. The dependent curve of emission intensity at

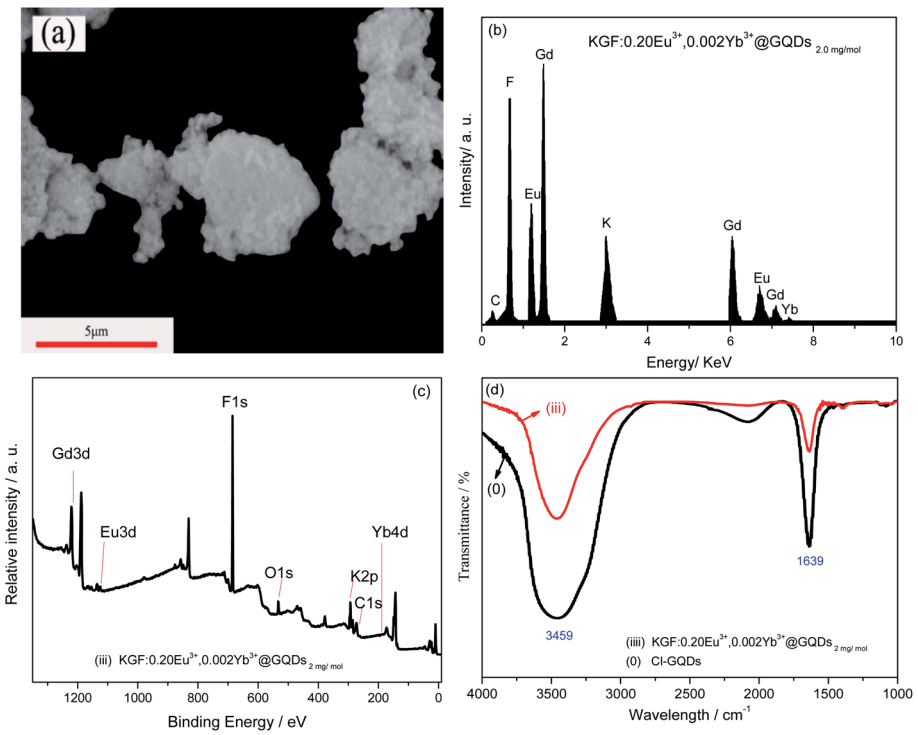

Fig. 2 SEM image, EDS, XPS and FTIR spectra of sample (iii), KGF:0.20Eu^{3+}, 0.002Yb^{3+}@GQDs$_{2\ mg\ mol^{-1}}$: (a) SEM, (b) EDS, (c) XPS, (d) FTIR.

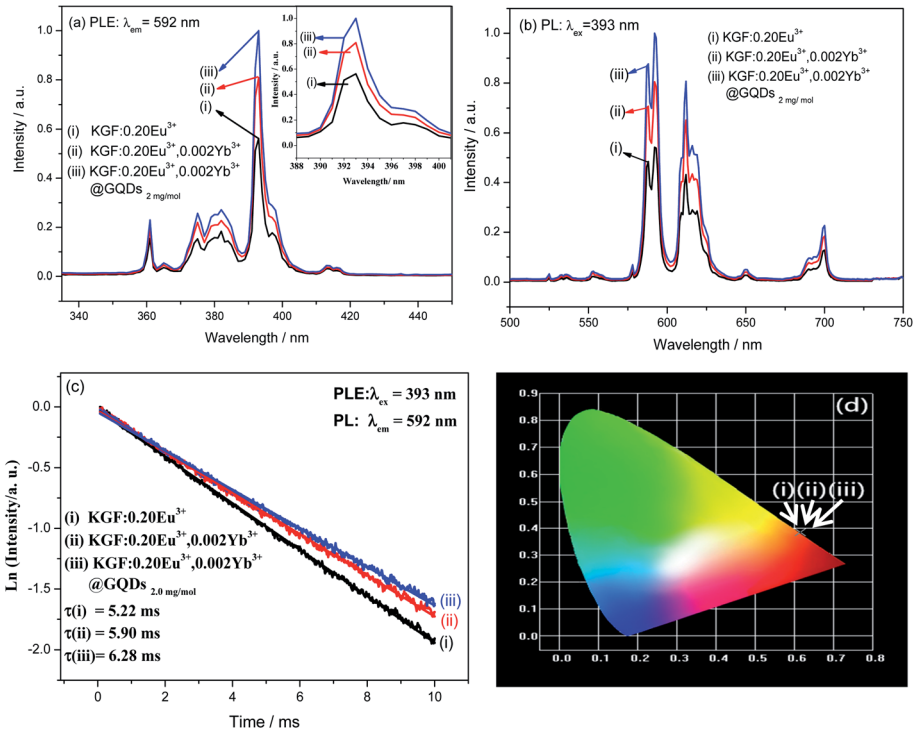

Fig. 3 Luminescent properties of three samples, (i) KGF:0.20Eu^{3+}; (ii) KGF:0.20Eu^{3+}, 0.002Yb^{3+}; (iii) KGF:0.20Eu^{3+}, 0.002Yb^{3+}@$GQDs_{2\ mg\ mol^{-1}}$: (a) PLE spectra, (b) PL spectra, (c) decay curves, (d) CIE chromaticity diagrams.

592 nm on different y is also a parabola, and it has a maximum when x is about 0.002.

Based on the result of Fig. 4b, the optimal double-doped sample (KGF:0.20Eu^{3+}, 0.002Yb^{3+}) was further coated with GQDs. The emission spectra (PL) of KGF:0.20Eu^{3+},0.002Yb^{3+}@$GQDs_z$ samples are shown in Fig. 4c. Fig. 4c shows that the PL intensity curve with different z is a parabola with a maximum value. The optimal concentration of GDQs for KGF:0.20Eu^{3+},0.002Yb^{3+}@$GQDs_z$ phosphors is 2 mg mol^{-1}. The results show that the obvious luminescent

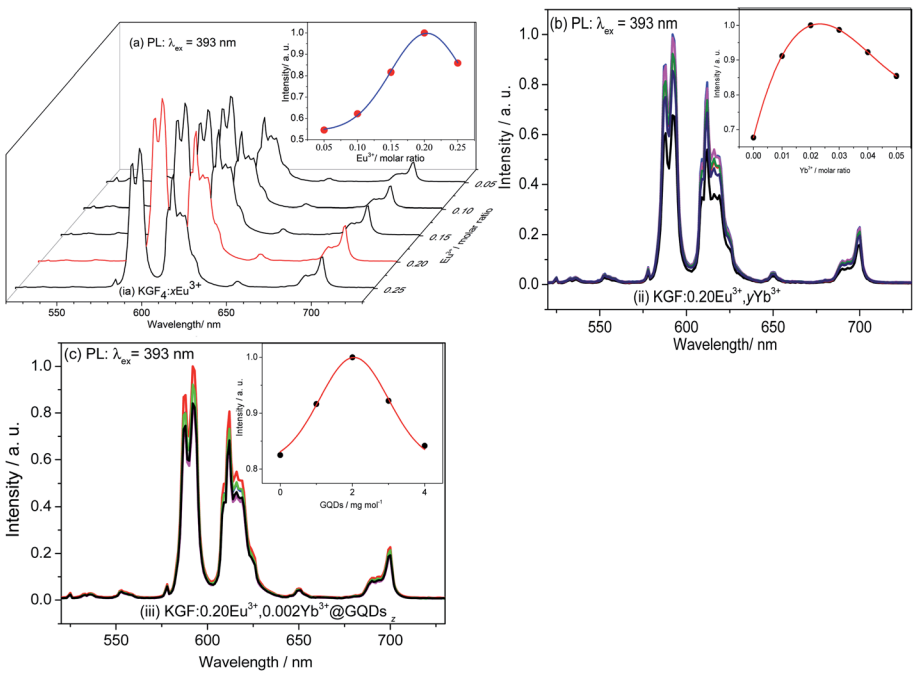

Fig. 4 Emission spectra of three samples: (a) PL spectra of KGF:xEu^{3+}; (b) PL spectra of KGF:0.20Eu^{3+},yYb^{3+}; (c) PL spectra of KGF:0.20Eu^{3+},0.002Yb^{3+}@$GQDs_{z(z=0-4)}$.

enhancement can be obtained by coating a small amount of GQDs.

3.4 Luminescent thermal stabilities

Luminescent thermal properties of the samples (i–iii) at different temperatures are shown in Fig. 5. Fig. 5a–c shows the integrated PL intensity curves of the three samples are strongly affected by temperature. Fig. 5d shows that the curve of the sample (i) is a nonlinear curve with monotonically decreasing, and curves of the sample (ii–iii) are parabolas, which is caused by the NTQ effect.[36,37] Fig. 5d further shows that curve (iii) is higher than curve (ii), indicates that the effect of the sample (iii) is stronger than that of the sample (ii). The highest points of the two parabola curves (curves (ii) and (iii)) are 130, 170 °C, which the corresponding integrated PL intensities are 117.7 and 156.5% of that initial value at 30 °C, respectively. So, the optimal sample (KGF:0.20Eu^{3+}, 0.002Yb^{3+}@GQDs$_{2\ mg\ mol^{-1}}$) has high luminescent thermal stability, due to the NTQ effect.

The results of Fig. 5d show that: (a) the sample (i) has no such the effect, but the sample (ii) has, indicating that the effect is induced by co-doping of Yb^{3+}. The effect induced by double doped ion was also observed in $LuVO_4$:Bi^{3+}, Eu^{3+} phosphor reported by Zhang *et al.*;[38] (b) the effect is further obviously enhanced when the surface of the double doped sample is coated with GQDs. The enhancement of the effect by GQDs was also occurred in GQDs coated Mn^{4+} doped fluoride red emitting phosphor.[40]

In previous work,[33] we have reported that $KGdF_4$:Eu^{3+}, Sm^{3+}@GQDs also has the NTQ effect, but their co-doping sample ($KGdF_4$:Eu^{3+},Sm^{3+}) has not. The results show that Eu^{3+} and different rare earth ions co-doped on the same matrix ($KGdF_4$) have different luminescent thermal properties, and only proper co-doping can obtain samples with the NTQ effect.

Mechanism of the effect has been discussed in some reports,[24,41–45] and was suggested that the electrons of phosphor gain energy supply from the electron trap produced by the defect of the matrix with the increase of temperature, and then the effect is induced.

In this paper, the mechanism of the effect is further explored from the perspective of energy conservation. The intensity of the excited light is constant whether at the parabola starting point or at its apex (Fig. 5d). However, the integrated PL intensity at the apex is stronger than that at the starting point. According to the mechanism reported in the literature, the extra energy required at the apex is provided by the electrons in the electron trap. From a macro point of view, in the whole variable temperature test system, the only way to provide extra energy is the thermal energy of the heating system. Therefore, it is not difficult to find that the energy in the electron trap is converted from the thermal energy. This mechanism can be represented with Fig. 5e and f. Fig. 5e and f show that: first, after double-doping of Yb^{3+} (Fig. 5e), the defects suitable for forming electron traps are formed in the matrix, and then the electrons are driven by heat and trapped by the defects, and finally the electrons transfer energy to the $^5L_6$ energy level of Eu^{3+} to resulting in the NTQ effect. In addition, when the double-doped sample is coated with GQDs (Fig. 5f), more defects are produced and more electrons are captured, so more energy is transferred to the $^5L_6$ energy level, which induces a stronger the NTQ effect. The mechanism of Fig. 5e and f is suggested as mechanism of energy conversion from heat to light.

3.5 Luminescent performances of prototype red light LEDs

The luminescent performances of the prototype red light LEDs are shown in Fig. 6. The LEDs were fabricated by coating mixture of the samples (i, iii) KGF:0.20Eu^{3+},

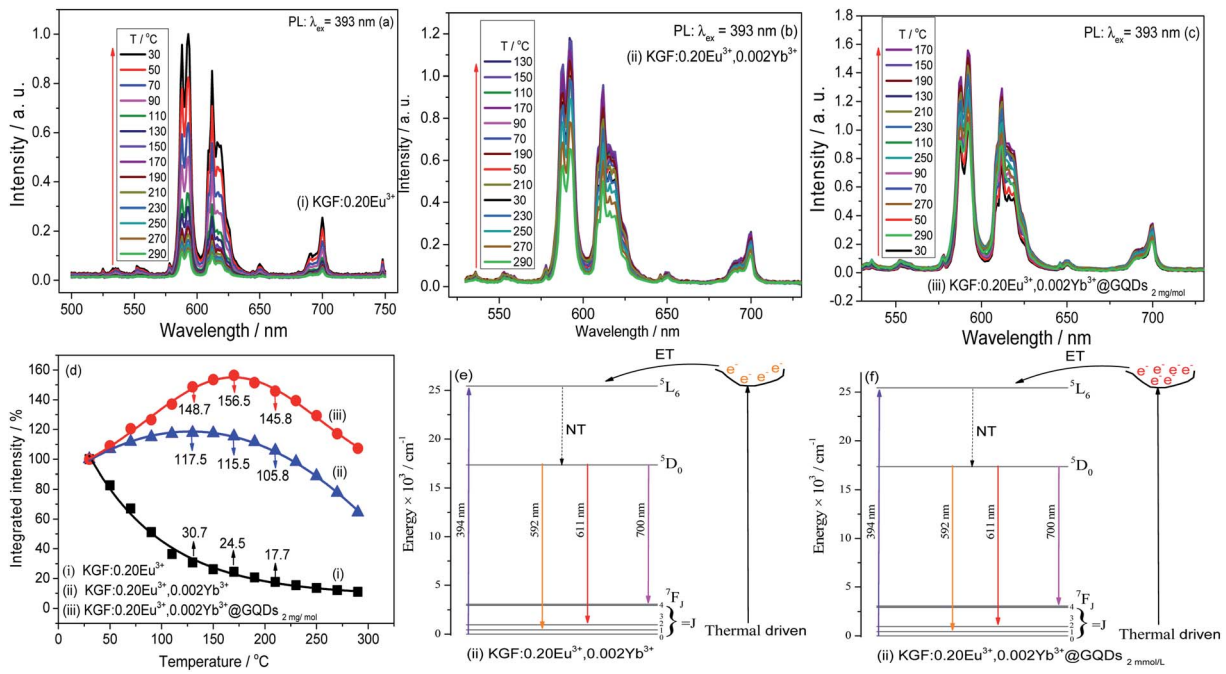

Fig. 5 Luminescent properties of three samples at different temperatures, (i) KGF:0.20Eu^{3+}; (ii) KGF:0.20Eu^{3+}, 0.002Yb^{3+}; (iii) KGF: 0.20Eu^{3+}, 0.002Yb^{3+}@GQDs$_{2\ mg\ mol^{-1}}$: (a–c) PL spectra, (d) integrated intensity curves, (e and f) mechanism of negative thermal quenching.

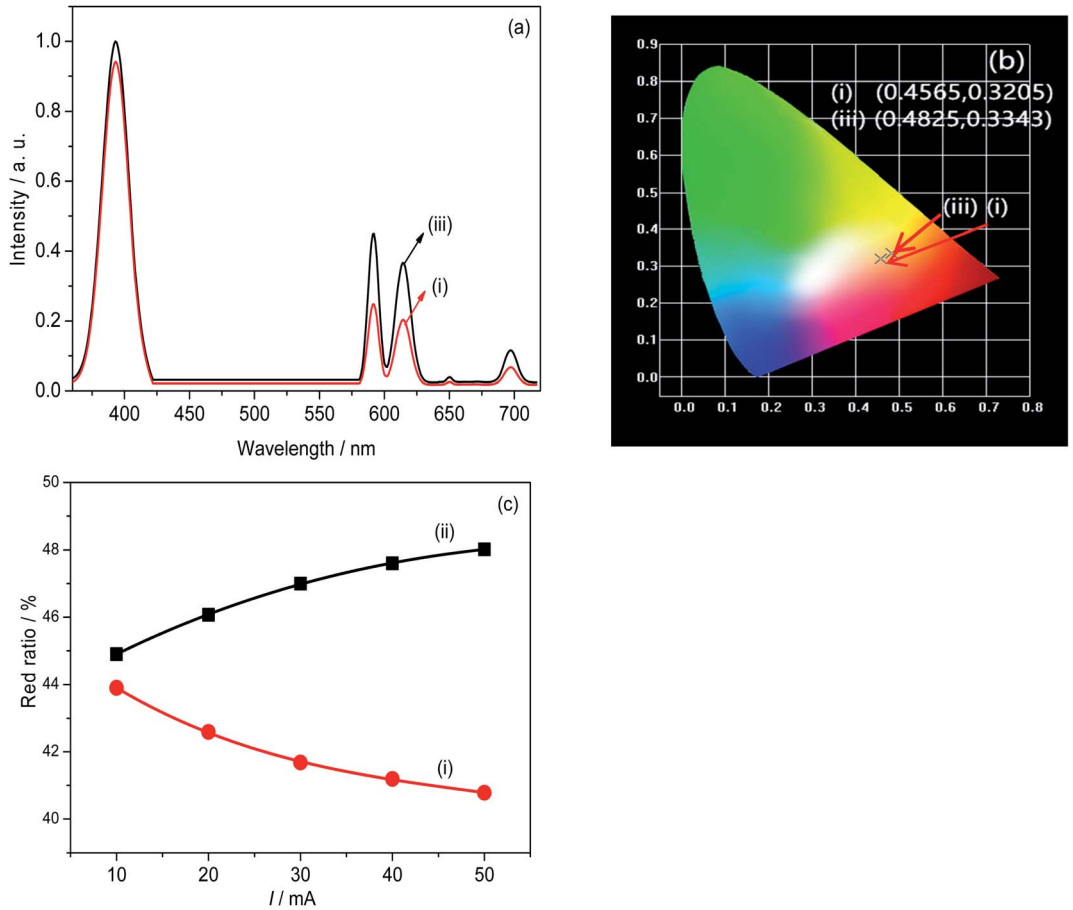

Fig. 6 Luminescent performances of prototype LEDs (samples (i, iii) + 395 nm UV chip), (i) KGF:0.20Eu^{3+}, (iii) KGF:0.20Eu^{3+}, 0.002Yb^{3+}@$GQDs_{2\ mg\ mol^{-1}}$: (a) electroluminescence spectrum under a 20 mA drive current, (b) CIE chromaticity diagram, (c) red ratio under a different drive current.

0.002Yb^{3+}@$GQDs_{2\ mg\ mol^{-1}}$ and epoxy onto a 395 nm UV chip and tested at different driving currents. Fig. 6a shows the electroluminescence spectra of the LEDs, which consist emissions of UV chip and the samples. Fig. 6b depicts CIE chromaticity diagrams of the LEDs, which are (0.5373, 0.3494) and (0.5163, 0.3392), respectively. Results of Fig. 6b indicate that the LEDs emit orange red light, which is supported by orange main emission (about 592 nm) in Fig. 3b.

The red color ratio of the LEDs at different driving currents is shown in Fig. 6c. Fig. 6c illustrates that the trend of the two curves is just the opposite. Curve (iii) increases with the increase of the driving current, while curve (i) decreases with the increase of the driving current. It is well known that the operating temperature of the chip increases with the increase of the driving current of the chip. It can be seen from the illustration in Fig. 5d, before 170 °C, curve (iii) monotonically rises with the increase of temperature, while curve (i) monotonically decreases with the increase of temperature. Obviously, the results of Fig. 6c are supported by results of Fig. 5d, and it can be further inferred that the operating temperature of the UV chip driven by 50 mA current does not exceed 170 °C. Furthermore, the results of Fig. 6c also indicate that the optimal sample (KGF: 0.20Eu^{3+}, 0.002Yb^{3+}@$GQDs_{2\ mg\ mol^{-1}}$) has high luminescent thermal stability, which can be applied for high power WLEDs.

4. Conclusions

In summary, a series of $KGdF_4$:Eu^{3+},Yb^{3+}@GQDs red emitting phosphor have been synthesized by co-precipitation method, and their luminescent thermal properties have also been studied. More intriguingly, the NTQ effect is formed induced by the double doping of Yb^{3+}, and the effect is further enhanced by GQDS coating. The strongest integrated PL intensities of the optimal double doped sample and the optimal GQDs coated sample are at 130 and 170 °C, which the corresponding integrated PL intensities are 117.7 and 156.5% of that initial value at 30 °C, respectively. The NTQ effect makes the optimal GQDs coated sample have good luminescent thermal stability. A mechanism of energy conversion from heat to light is suggested for the NTQ effect.

Conflicts of interest

The authors declare that they have no conflict of interest.

Author contributions

Zhigao Wu: methodology, formal analysis, investigation, writing – original draft. Chang Chen: investigation. Yaxiong

Wang: investigation. Chaolian Luo: investigation. Sen Liao: conceptualization, supervision. Yingheng Huang: review & editing, visualization. Junyu Ming: review & editing, visualization.

Acknowledgements

This research is supported by the National Natural Science Foundation of China (Grant No. 21661006 and 21965004), the Natural Science Foundation of Guangxi Zhuang Autonomous Region, China (Grant No. 2019GXNSFDA245022), the Scientific Research Foundation of Guangxi University (Grant No. XDZ140116), the Innovation Project of Guangxi Graduate Education (Grant No. YCSW2020015), the Students Experimental Skills and Innovation Ability Training Fund Project of Guangxi University (No. 202010593186).

References

1 P. Du, X. Y. Huang and J. S. Yu, Facile synthesis of bifunctional Eu^{3+}-activated $NaBiF_4$ red-emitting nanoparticles for simultaneous white light-emitting diodes and field emission displays, *Chem. Eng. J.*, 2017, **337**, 91–100.

2 S. S. Liang, M. M. Shang, H. Z. Liang, K. Li, Y. Zhang and J. Lin, Deep red MGe_4O_9:Mn^{4+} (M = Sr, Ba) phosphors: structure, luminescence properties and application in warm white light emitting diodes, *J. Mater. Chem. C*, 2016, **426**, 6409–6416.

3 A. J. Huang, Z. W. Yang, C. Y. Yu, Z. Z. Chai, J. B. Qiu and Z. G. Song, Tunable and white light emission of a single-phased $Ba_2Y(BO_3)_2Cl$: Bi^{3+}, Eu^{3+} phosphor by energy transfer for ultraviolet converted white LEDs, *J. Phys. Chem. C*, 2017, **121**, 5267–5276.

4 J. H. Zheng, S. Q. Wu, G. Chen, S. J. Dang, Y. X. Zhuang, Z. Q. Guo, Y. J. Lu, Q. J. Cheng and C. Chen, Blue-emitting $Ca_5(PO_4)_3Cl$:Eu^{2+} phosphor for near-UV pumped light emitting diodes: Electronic structures, luminescence properties and LED fabrications, *J. Alloys Compd.*, 2016, **663**, 332–339.

5 G. Annadurai and S. Masilla Moses Kennedy, Synthesis and photoluminescence properties of $Ba_2CaZn_2Si_6O_{17}$:Eu^{3+} red phosphors for white LED applications, *J. Lumin.*, 2016, **169**, 690–694.

6 H. Guo, X. Y. Huang and Y. J. Zeng, Synthesis and photoluminescence properties of novel highly thermal-stable red-emitting $Na_3Sc_2(PO_4)_3$:Eu^{3+} phosphors for UV-excited white-light-emitting diodes, *J. Alloys Compd.*, 2018, **741**, 300–306.

7 Z. Jia, X. L. Zhang, X. Y. Hua, Y. Dong, H. L. Li, C. Q. Feng, Y. G. Wang and M. J. Xia, Engineering mixed polyanion red-emitting $Rb_2Bi(PO_4)(WO_4)$:Eu^{3+} phosphors with negligible thermal quenching and high quantum yield, *J. Alloys Compd.*, 2020, **844**, 155875.

8 K. Li and R. V. Deun, Eu^{3+}/Sm^{3+}-doped $Na_2BiMg_2(VO_4)_3$ from substitution of Ca^{2+} by Na+and Bi^{3+} in $Ca_2NaMg_2(VO_4)_3$: Color-tunable luminescence *via* efficient energy transfer from $(VO_4)^{3-}$ to Eu^{3+}/Sm^{3+} ions, *Dyes Pigm.*, 2018, **155**, 258–264.

9 M. E. Alvarez-Ramosa, R. C. Carrillo-Torresa, R. Sánchez-Zeferinoa, U. Caldiñob and J. Alvarado-Rivera, Co-emission and energy transfer of Sm^{3+} and/or Eu^{3+} activated zincgermanate-tellurite glass as a potential tunable orange to reddish-orange phosphor, *J. Non-Cryst. Solids*, 2019, **521**, 119462.

10 Z. X. Fu and B. R. Liu, Hydrothermal synthesis, energy transfer and luminescence enhancement of rhombohedral LaOF: Sm^{3+}-Eu^{3+} nanoparticles, *Phys. B*, 2019, **574**, 311653.

11 X. G. Zhang, J. L. Zhang, Y. B. Chen and M. L. Gong, Energy transfer and multicolor tunable emission in single-phase Tb^{3+}, Eu^{3+} co-doped $Sr_3La(PO_4)_3$ phosphors, *Ceram. Int.*, 2016, **42**, 13919–13924.

12 B. Li, X. Huang, H. Guo and Y. Zeng, Energy transfer and tunable photoluminescence of $LaBWO_6$:Tb^{3+}, Eu^{3+} phosphors for near-UV white LEDs, *Dyes Pigm.*, 2018, **150**, 67–72.

13 G. T. Xiang, Y. Ma and W. Liu, Enhancement of Eu^{3+} red upconversion in Lu_2O_3 : Yb^{3+}/Eu^{3+} powders under the assistance of bridging function originated from Ho^{3+} tridoping, *Inorg. Chem.*, 2017, **56**, 13955–13961.

14 N. Rakova, S. C. Duartea and G. S. Maciel, Evaluation of the energy transfer mechanism leading to tunable green-to-red cooperative up-conversion emission in Eu^{3+}-Yb^{3+} co-doped CaF_2 powders, *J. Lumin.*, 2019, **214**, 116561.

15 S. K. Ranjan, A. K. Soni and V. K. Rai, Frequency upconversion and fluorescence intensity ratio method in Yb^{3+}-ion-sensitized Gd_2O_3:Er^{3+}-Eu^{3+} phosphors for display and temperature sensing, *Methods Appl. Fluoresc.*, 2017, **5**, 035004.

16 X. X. Han, E. H. Song, W. B. Chen, Y. Y. Zhou and Q. Y. Zhang, Color-tunable upconversion luminescence and prolonged Eu^{3+} fluorescence lifetime in fluoride $KCdF_3$: Yb^{3+},Mn^{2+},Eu^{3+} *via* controllable and efficient energy transfer, *J. Mater. Chem. C*, 2020, **8**, 9836–9844.

17 T. K. Pathak, A. Kumar, L. J. B. Erasmus, A. Pandey, E. Coetsee, H. C. Swart and R. E. Kroon, Highly efficient infrared to visible up-conversion emission tuning from red to white in Eu/Yb co-doped $NaYF_4$ phosphor, *Spectrochim. Acta, Part A*, 2019, **207**, 23–30.

18 H. F. Guo, Q. F. Shi, K. V. Ivanovskikh, L. Wang, C. Cui and P. Huang, A high color purity red-emission phosphor based on Sm^{3+} and Eu^{3+} co-doped $Ba_3Bi(PO_4)_3$, *Mater. Res. Bull.*, 2020, **126**, 110836.

19 P. Ranjith, S. Sreealsa, J. Tyagi, K. Jayanthi, G. Jagannath, P. Patra, S. Ahmad, K. Annapurna, A. R. Allu and S. Das, Elucidating the structure and optimising the photoluminescence properties of $Sr_2Al_3O_6F$: Eu^{3+} oxyfluorides for cool white-LEDs, *J. Alloys Compd.*, 2020, **826**, 154015.

20 L. Zhao, F. Y. Fan and X. Chen, Luminescence and thermal-quenching properties of silicate-based red-emitting $K_4CaSi_3O_9$:Eu^{3+} phosphor, *J. Mater. Sci.: Mater. Electron.*, 2018, **29**, 5975–5981.

21 Z. J Zhang, L. L. Sun and B. Devakumar, Synthesis and photoluminescence properties of a new blue-light-excitable red phosphor $Ca_2LaTaO_6:Eu^{3+}$ for white LEDs, *J. Lumin.*, 2020, **222**, 117173.

22 S. Y. Xin, F. G. Zhou and L. Zhao, Synthesis, Luminescence Property and Thermal Quenching Investigation of Niobate Phosphors $Ba_3ZrNb_4O_{15}:Eu^{3+}$under Multiple Excitations, *ECS J. Solid State Sci. Technol.*, 2018, **7**, R94–R98.

23 D. Zhao, Y. L. Xue and S. R. Zhang, Non-concentration quenching, good thermal stability and high quantum efficiency of $K_5Y(P_2O_7)_2:Eu^{3+}/Tb^{3+}$ phosphors with a novel two-dimensional layer structure, *J. Mater. Chem. C*, 2019, **7**, 14264–14274.

24 G. Zhu, Z. W. Li, X. J. Wang, F. G. Zhuo, M. Gao, S. Y. Xin and Y. H. Wang, Highly Eu^{3+} ions doped novel red emission solid solution phosphors $Ca_{18}Li_3$(Bi, Eu) $(PO_4)_{14}$: structure design, characteristic luminescence and abnormal thermal quenching behavior investigation, *Dalton Trans.*, 2019, **48**, 1624–1632.

25 W. J. Zhang, Y. Wang and X. X. Zhang, The effect of graphene oxide concentration on luminescence property of Tb^{3+}-complexes, *J. Inorg. Organomet. Polym. Mater.*, 2018, **28**, 2596–2602.

26 Y. M. Liu, Y. L. Li and Y. T. Feng, Effects of graphene quantum dots coating on the luminescence properties of $K_2SiF_6:Mn^{4+}$ red-emitting phosphors, *J. Mater. Sci.: Mater. Electron.*, 2020, **31**, 444–456.

27 A. Prasad, A. S. Rao and G. V. Prakash, A study on up-conversion and energy transfer kinetics of $KGdF_4:Yb^{3+}/Er^{3+}$ nanophosphors, *J. Mol. Struct.*, 2020, **1205**, 127647.

28 A. Prasad, A. S. Rao, M. Gupta and G. V. Prakash, Morphological and luminescence studies on $KGdF_4:Yb^{3+}/Tb^{3+}$ up-conversion nanophosphors, *Mater. Chem. Phys.*, 2018, **219**, 13–21.

29 J. P. Ma, C. Yi and C. Li, Facile synthesis and functionalization of color-tunable Ln^{3+}-doped $KGdF_4$ nanoparticles on a microfluidic platform, *Mater. Sci. Eng.*, 2020, **108**, 110381.

30 A. Prasad, A. S. Rao and G. V. Prakash, Up-conversion luminescence and EPR properties of $KGdF_4:Yb^{3+}/Tm^{3+}$ nanophosphors, *Optik*, 2020, **208**, 164538.

31 Y. Y. Bu and X. H. Yan, Temperature dependent photoluminescence of Eu^{3+}-doped $Ca_7V_4O_{17}$, *J. Lumin.*, 2017, **190**, 50–55.

32 S. D. Li, Q. Y. Meng and S. C. Lü, Study on optical temperature sensing properties of Tb^{3+}, Eu^{3+} co-doped $CaMoO_4$ phosphor, *J. Lumin.*, 2018, **200**, 103–110.

33 J. Y. Ming, Y. X. Wang, S. K. Ling, S. Liao, Y. H. Huang and H. X. Zhang, Conversion of thermal energy to light energy and energy transfer in $KGdF_4$: Eu^{3+},Tb^{3+} phosphors, *Inorg. Chem. Commun.*, 2021, **127**, 108549.

34 N. Duan, H. Zhang, Y. Nie, S. J. Wu, T. T. Miao, J. Chen and Z. P. Wang, Fluorescence resonance energy transfer-based aptamer biosensors for bisphenol a using lanthanide-doped $KGdF_4$ nanoparticle, *Anal. Methods*, 2015, **7**, 5186–5192.

35 P. V. Do, V. X. Quang, L. D. Thanh, V. P. Tuyen, N. X. Ca, V. X. Hoa and H. V. Tuyen, Energy transfer and white light emission of $KGdF_4$ polycrystalline co-doped with Tb^{3+}/Sm^{3+} ions, *Opt. Mater.*, 2019, **92**, 174–180.

36 C. Y. Cao, H. M. Noh, B. K. Moon, B. C. Choi and J. H. Jeong, Synthesis and optical properties of Ce^{3+}/Tb^{3+} doped LaF_3, $KGdF_4$, and KYF_4 nanocrystals, *J. Lumin.*, 2014, **152**, 206–209.

37 D. M. Yang, G. G. Li, X. J. Kang, Z. Y. Cheng, P. A. Ma, C. Peng, H. Z. Lian, C. X. Li and J. Lin, Room temperature synthesis of hydrophilic Ln^{3+}-doped $KGdF_4$ (Ln = Ce, Eu, Tb, Dy) nanoparticles with controllable size: energy transfer, size-dependent and color-tunable luminescence properties, *Nanoscale*, 2012, **4**, 3450–3459.

38 C. Y. Cao, H. K. Yang, J. W. Chung, B. K. Moon, B. C. Choi, J. H. Jeong and K. H. Kim, Hydrothermal synthesis and enhanced photoluminescence of Tb^{3+} in Ce^{3+}/Tb^{3+} doped $KGdF_4$ nanocrystals, *J. Mater. Chem.*, 2011, **21**, 10342–10347.

39 Y. C. Zhao, L. J. Huang, Y. X. Wang, J. G. Tang, Y. Wang, J. X. Liu, L. A. Belfiore and M. J. Kipper, Synthesis of graphene oxide/rare-earth complex hybrid luminescent materials *via* π–π stacking and their pH-dependent luminescence, *J. Alloys Compd.*, 2016, **687**, 95–103.

40 E. H. Song, J. Q. Wang, S. Ye, X. F. Jiang, M. Y. Peng and Q. Y. Zhang, Room-temperature synthesis and warm-white LED applications of Mn^{4+} ion doped fluoroaluminate red phosphor Na_3AlF_6: Mn^{4+}, *J. Mater. Chem. C*, 2016, **4**, 2480–2487.

41 E. H. Song, J. Q. Wang, J. H. Shi, T. T. Deng, S. Ye, M. Y. Peng, J. Wang, L. Wondraczek and Q. Y. Zhang, Highly efficient and thermally stable $K_3Al_6:Mn^{4+}$ as a red phosphor for ultra-high-performance warm white light-emitting diodes, *ACS Appl. Mater. Interfaces*, 2017, **9**, 8805–8812.

42 Z. G. Zhang, Z. P. Zhu, Z. Y. Guo, F. W. Mo and Z. C. Wu, A zero-thermal-quenching and color-tunable phosphor $LuVO_4$: Bi^{3+}, Eu^{3+} for NUV LEDs, *Dyes Pigm.*, 2018, **156**, 67–73.

43 Y. L. Li, X. Zhong, Y. Yu, Y. M. Liu, S. Liao, Y. H. Huang and H. X. Zhang, H_2O_2-free preparation of $K_2SiF_6:Mn^{4+}$ and remarkable high luminescent thermal stability induced by coating with graphene quantum dots, *Mater. Chem. Phys.*, 2021, **260**, 124149.

44 S. Q. Fang, T. C. Lang, T. Hao, J. Y. Wang, J. Y. Yang, S. X. Cao, L. L. Ping, B. T. Liu, A. N. Yakovlev and V. I. Korepanov, Zero-thermal-quenching of Mn^{4+} far-red-emitting in $LaAlO_3$ perovskite phosphor *via* energy compensation of electrons' traps, *Chem. Eng. J.*, 2020, **389**, 124297.

45 X. C. Wang, Z. Y. Zhao, Q. S. Wu, C. Wang, Q. Wang, Y. Y. Li and Y. H. Wang, Structure, photoluminescence and abnormal thermal quenching behavior of Eu^{2+}-doped $Na_3Sc_2(PO_4)_3$: a novel blue-emitting phosphor for n-UV LEDs, *J. Mater. Chem. C*, 2016, **4**, 8795–8801.